Surface tension and orthobaric densities for vibrating square well dumbbells. I

ARTICLE *in* THE JOURNAL OF CHEMICAL PHYSICS · MARCH 2010

Impact Factor: 2.95 · DOI: 10.1063/1.3350531 · Source: PubMed

2 AUTHORS, INCLUDING:

Jose Alejandre
Metropolitan Autonomous University
81 PUBLICATIONS **2,248** CITATIONS

Surface tension and orthobaric densities for vibrating square well dumbbells. I

Gustavo A. Chapela[1,a] and José Alejandre[2]
[1]*Departamento de Física, Universidad Autónoma Metropolitana-Iztapalapa, Av. San Rafael Atlixco 186, Col. Vicentina, 09340 México Distrito Federal Mexico*
[2]*Departamento de Química, Universidad Autónoma Metropolitana-Iztapalapa, Av. San Rafael Atlixco 186, Col. Vicentina, 09340 México Distrito Federal Mexico*

(Received 15 October 2009; accepted 9 February 2010; published online 10 March 2010)

Surface tensions and liquid-vapor orthobaric densities are calculated for a wide variety of vibrating square well dumbbells using discontinuous molecular dynamics simulations. The size of the vibration well, the elongation or bond distance of the two particles of the dumbbell, the asymmetry in size (and interaction range) of the two particles, and the depth of the interaction well are the variables whose effects are systematically evaluated in this work. Extensive molecular dynamics simulations were carried out and the orthobaric liquid-vapor densities are compared with those obtained previously by other authors using different methods of simulation for rigid and vibrating square well dumbbells. Surface tension values are reported for the first time for homonuclear and heteronuclear vibrating square well dumbbells as well as for all the simulated series. The molecular dynamics results of tangent homonuclear dumbbells are compared with those from Monte Carlo simulations also obtained in this work, as a way of checking the order of magnitude of the molecular dynamics results. The size of the vibration well is shown to have a small influence on the resulting properties. Decreasing elongation and the size of the second particle increase critical temperatures, liquid densities, and surface tensions. Moderate increases in the depth of the interaction well have the same effect. For larger asymmetries of the depth of the interaction well on the dumbbell particles, a strong association phenomenon is observed and the main effects are a maximum on the critical temperature for increasing well depth and a decrease in the surface tension. © *2010 American Institute of Physics*. [doi:10.1063/1.3350531]

I. INTRODUCTION

The square well diatomic (SWD) is a simple model of molecular interactions having both repulsive and attractive potentials. Monte Carlo (MC) simulations represent this model as two spheres separated by a fixed distance and discontinuous molecular dynamics (DMD) treats it as a vibrating SWD (VSWD). Both particles are trapped in an intramolecular square well, which keeps them rattling or vibrating together. The main aim of this work is to present a systematic study of the behavior of VSWD to calculate orthobaric densities and surface tensions. Orthobaric densities for some systems have already been reported but there are no surface tension data published. The systematic study is based on some variables that account for the shape and the interaction of the molecules. The size of the vibrating well L_{vw} is the first variable selected. The elongation L (the distance between the centers of the particles) and the relative size of the second particle σ_2 are variables considered also in this study. The relative depth of the interacting square well of the second sphere ϵ_2 is used as the fourth variable taken into account. The diameter and the well depth of the first particle are kept constant for all series considered ($\sigma_1=1$ and $\epsilon_1=1$). Some of the series presented here show a strong association, and using a combination of the last three variables mentioned allows us to cover the range from VSWD to associating fluids[1,2] passing through a patchy model having just one patch.[3,4] A systematic study of associating phenomena will be the subject of a separate paper that will be submitted shortly.

DMD has been used since the initial work for hard spheres by Alder *et al.*[5] to study simple fluids that have complex physical behaviors. This procedure was extended to chains of spheres interacting with a square well potential by Rapaport.[6,7] MC simulations of hard core chains were performed by Tildesley *et al.*,[8] which obtained an equation of state for these series based on the calculated contact radial distribution functions. DMD simulations were applied to different forms of molecules by Chapela *et al.*[9,10] Extensive DMD, MC, and Gibbs ensemble simulations were performed by Hall and co-workers[11–13] for SWDs and its mixtures. They compared their results against the equation of state obtained by integral equations and perturbation theory. The liquid-vapor equilibrium of square well chains of different elongations and number of particles in the chain were studied by Elliot and co-workers.[14,15] MC simulations by Escobedo *et al.*[16,17] were performed for homonuclear SWD and homonuclear chains up to 100 tangent segments interacting with a SW potential. Kim *et al.*[18] performed MC simulations for SWD at different attraction ranges of the SW. Lisal *et al.*[19] studied homonuclear and heteronuclear SWDs. The data ob-

[a]Author to whom correspondence should be addressed. Electronic mail: gchapela@xanum.uam.mx.

tained with these computer simulations have been used to test perturbation[11,13,20] and integral equation theories.[13,21–24] The calculation of surface tension at the liquid-vapor interface of SWD has been reported using density functional theories[14,25] but, to the best of our knowledge, this is the first time this property is calculated using simulation methods.

One of the main tasks of the molecular simulation community has been to compare and determine if the results obtained with the MD and MC algorithms for the same systems are equivalent, or if not, to explain the differences. As mentioned above, DMD and MC had been used to simulate molecular systems interacting with discontinuous potentials. In the case of the SWD, the results from these two methods (SWD via MC and VSWD via DMD) have been compared without knowing precisely how much do they differ. The existence of the vibrating well in the VSWD, compared to a delta function at a fixed distance in the SWD, makes the two molecular arrays different. This work sets out to test the hypothesis that they have equivalent orthobaric densities and surface tensions provided that the range of the vibrating well is kept small. The two methods use similar computing time in the simulations. MC has the advantage of been able to simulate both SWD and VSWD. DMD has the ability to calculate dynamical properties and has also, by virtue of the intramolecular potentials, the flexibility to represent many different shapes of molecules[9] and to simulate them using the same code. The use of the virial route to obtain the surface tension is natural to this simulation method.[26] Displacing complex molecules by MC techniques requires procedures like the one put forward by Escobedo *et al.*[17]

This work is organized as follows: in Sec. II the molecular model and interaction potential are given, Sec. III includes a brief discussion of the DMD simulation method, Sec. IV gives an account of the thermodynamic properties calculated, Sec. V describes the simulated series in detail, Sec. VI presents the results, followed by a discussion of the main conclusions in Sec. VII. References and acknowledgments are included at the end.

II. MOLECULAR MODEL AND INTERACTION POTENTIAL

The VSWD is the model chosen in this work to represent a simple molecular system that shows a complex behavior. Figure 1 depicts a VSWD, where all the variables relevant to this work are pictorially defined. The only difference between SWD and VSWD is the intramolecular potential, a fixed distance for SWD and a SW potential with infinitely high walls for VSWD, to keep the particles in a molecule from drifting apart. This well is necessary to perform DMD on VSWD and one of the aims of this work is to assess the differences between these two models.

The interaction between two particles a and b is given by the following potential:

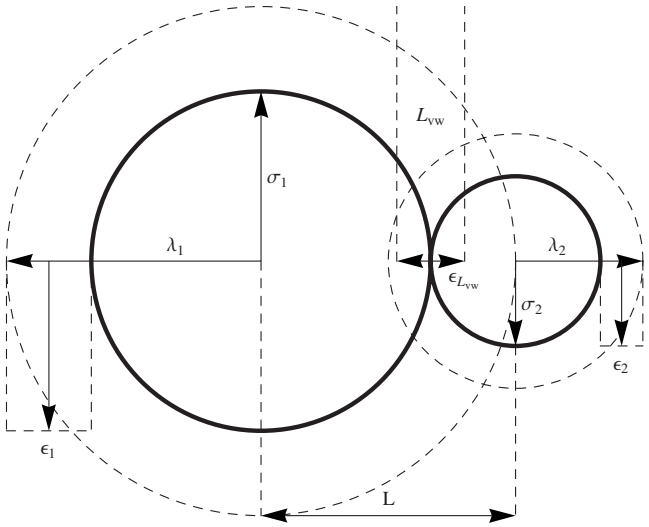

FIG. 1. Pictorial definition of the variables used. L_{vw}, L, σ_1, σ_2, ϵ_1, ϵ_2, λ_1, λ_2, and $\epsilon_{L_{vw}}$. In this work, $\sigma_1=1$, $\epsilon_1=1$, $\lambda_1=\lambda\sigma_1$, $\lambda_2=\lambda\sigma_2$, with $\lambda=1.5$ and $\epsilon_{L_{vw}}=0$.

$$U(r_{ab}) = \begin{cases} \text{Intra} & \\ \infty, & r_{ab} \leqslant L - L_{vw}/2 \\ \epsilon_{L_{vw}}, & L - L_{vw}/2 < r_{ab} \leqslant L + L_{vw}/2 \\ \infty, & r_{ab} > L + L_{vw}/2 \\ \text{Inter} & \\ \infty, & r_{ab} \leqslant \sigma_{ab} \\ -\epsilon_{ab}, & \sigma_{ab} < r_{ab} \leqslant \lambda_{ab} \\ 0, & r_{ab} > \lambda_{ab}, \end{cases} \tag{1}$$

where r_{ab} is the distance between particles a and b, $\sigma_{ab}=(\sigma_a+\sigma_b)/2$ and $\epsilon_{ab}=\sqrt{\epsilon_a\epsilon_b}$ are the diameter and energy parameters obtained applying Lorentz–Berthelot rules, and $\lambda_{ab}=(\lambda_a+\lambda_b)/2$ is the range of the SW potential. The intramolecular interaction potential [top part of Eq. (1)] between two particles a and b in the same molecule (the vibrating well) is given by a SW of range L_{vw} centered at L, the elongation of the molecule. The depth of the well $\epsilon_{L_{vw}}=0$ for all cases considered in this work. The intermolecular interaction potential [bottom part of Eq. (1)] between two particles a and b in different molecules is given by a SW of size $\lambda_{ab}=\lambda\sigma_{ab}$ with a depth of the well ϵ_{ab}. In this work, a generic constant $\lambda=1.5$ is used and $\lambda_a=\lambda\sigma_a$ and $\lambda_b=\lambda\sigma_b$. In heteronuclear SWDs, when $\sigma_b\rightarrow 0\Rightarrow\lambda_b\rightarrow 0$, the model becomes one of associating molecules.[27]

III. DISCONTINUOUS MOLECULAR DYNAMICS

DMD is the chosen procedure to carry out the simulations of the model system described in Sec. IV. Rapaport[6] gave a detailed account of the procedure to simulate molecular shapes, where the particles are kept within the molecule with strings attached to every pair. Chapela *et al.*[9] used trapping wells as intramolecular potentials in order to achieve the same purpose. A brief account of the second approach is presented here.

Given the initial positions and velocities of the system of N molecules, the collision times are calculated for each pair.

The smallest time is selected and the particles are moved at a constant velocity to the collision position. Once there the collision between two particles is solved and the new velocities are obtained. Collision times for the two particles that just collided are calculated again and the process is started again. Time saving schemes, such as neighbor list and maximum collision time to keep this list as short as possible, are employed.

Liquid-vapor interface simulations are performed using a parallelepiped box with periodic boundary conditions in three directions. The molecules initially fill the simulation cell at a density within the unstable region of the phase diagram. A fast phase separation is observed after several thousands of collision and a liquid slab surrounded by vapor is formed.

IV. CALCULATED PROPERTIES

Equations to calculate pressure, vapor pressure, surface tension, density profiles, orthobaric densities, and critical points are given. Expressions for pressure and surface tension are given for both methods, DMD and MC.

A. DMD pressure and surface tension

Pressure is obtained using the Clausius' virial theorem,[1,28]

$$\langle P\rangle = \rho k_B T + \frac{1}{3Vt}\sum_{\text{col's}} m_i \Delta \mathbf{v}_{ij}\cdot \mathbf{r}_{ij}, \tag{2}$$

where $\langle P\rangle$ is the time average pressure, ρ is the atomic number density, k_B is the Boltzmann constant, and T is the temperature. The total elapsed simulation time t, which is the sum of individual times of each collision performed, m is the mass of the particles, $\Delta \mathbf{v}_{ij}$ is the velocity difference vector of the colliding pair of particles i and j before and after the collision, and $\mathbf{r}_{ij}$ is the vector joining the centers of the two atoms. The $\Sigma_{i,j}$ run through the total number of collision times. $\langle\cdots\rangle$ means time average.

The components of the pressure tensor are obtained using the Clausius' virial theorem as given in

$$\langle P_{xx}\rangle = \rho k_B T + \frac{1}{Vt}\sum_{\text{col's}} m_i \Delta v x_{ij} x_{ij}, \tag{3}$$

where P_{xx} is the instantaneous xx diagonal component of the pressure tensor, V is the system volume, $\Delta v x_{ij}$ is the x component of the velocity difference vector of the colliding pair of particles i and j before and after the collision, and x_{ij} is the x component of the vector joining the centers of the two atoms.

The surface tension of a planar interface was calculated using the mechanical definition of the atomic pressure tensor,[28,33]

$$\gamma = \frac{L_x}{2}\left[\langle P_{xx}\rangle - \frac{1}{2}(\langle P_{yy}\rangle + \langle P_{zz}\rangle)\right], \tag{4}$$

where $P_{\alpha\alpha}$ are the diagonal components of the pressure tensor and L_x is the length of the simulation box in the x direction. The factor $1/2$ outside of the square brackets is to average the surface tension of the two interfaces in the system. Care must be taken to avoid finite size effects by choosing a box large enough to have a surface area (area of the box parallel to the interface) of at least 10 atomic diameters.[29–32] The vapor pressure is obtained as the time average of the pressure tensor component normal to the interface $P_v = \langle P_{xx}\rangle$.

B. MC pressure and surface tension

In MC the surface tension is calculated using Eq. (4) but the instantaneous component P_{xx} of the pressure tensor is calculated using the molecular version given by

$$P_{xx} = \rho_m k_B T + \frac{1}{V}\sum_i \sum_{j>i} \mathbf{F}_{ij}\cdot \mathbf{R}_{ij}, \tag{5}$$

where ρ_m is the molecular density and $\mathbf{R}_{ij} = \mathbf{R}_i - \mathbf{R}_j$ with $\mathbf{R}_i$ as the center of mass position of molecule i. The force between particles i and j at a distance $\mathbf{r}_{ij}$ in two different molecules is

$$\mathbf{F}_{ij} = -\frac{\partial u(r_{ij})}{\partial r_{ij}}\frac{\mathbf{r}_{ij}}{r_{ij}}, \tag{6}$$

where for discontinuous potentials,[33,34]

$$\frac{\partial u(r_{ij})}{\partial r_{ij}} = -k_B T \delta(r_{ij} - r_\sigma), \tag{7}$$

where r_σ stands for every discontinuity of the intermolecular potential. The delta function was evaluated numerically,

$$\delta(r_{ij} - r_\sigma) = \frac{\Theta(r - r_\sigma) - \Theta(r - [r_\sigma + \Delta r_\sigma])}{\Delta r_\sigma}, \tag{8}$$

where $\Theta(x)$ is the step function and Δr_σ is an arbitrary distance from r_σ. The approximation in Eq. (8) is valid when $\Delta r_\sigma \to 0$.

The components of the pressure tensor were calculated as $P_{xx} = P_{xx}(r_\sigma^+) + P_{xx}(\lambda r_\sigma^-) + P_{xx}(\lambda r_\sigma^+)$. The procedure to calculate $\delta(r_{ij} - r_\sigma)$ was the same as that used for the spherical case.[35] $P_{xx}(r_\sigma^+)$ is obtained by summing distances over pairs at $r_\sigma < r_{ij} < r_\sigma + \Delta r_\sigma$, $P_{xx}(\lambda r_\sigma^-)$ for distances $(\lambda r_\sigma - \Delta r_\sigma) \leqslant r_{ij} \leqslant \lambda r_\sigma$, and $P_{xx}(\lambda r_\sigma^+)$ for distances $\lambda r_\sigma \leqslant r_{ij} \leqslant (\lambda r_\sigma + \Delta r_\sigma)$. The components P_{yy} and P_{zz} were obtained in the same way as P_{xx}. Values of the arbitrary distance $\Delta r_\sigma/\sigma_1 = 0.005$, 0.01, 0.02, 0.03, and 0.04 were used to calculate $\delta(r_{ij} - r_\sigma)$. At the end of the simulation, the components of the pressure tensor were extrapolated to $\Delta r_\sigma \to 0$ by using a linear regression. There are alternative ways to obtain the surface tension using MC simulations[26] without calculating the components of the pressure tensor, as done here with this δ function procedure.

C. Density profile

The density profile is

$$\rho(x) = \frac{\langle N(x, x + \Delta x)\rangle}{\Delta V}, \tag{9}$$

where $\langle N(x, x+\Delta x)\rangle$ is the average number of particles with positions between x and $x+\Delta x$ and ΔV is the volume of a slab. The liquid and vapor coexisting densities were obtained

TABLE I. Description of the simulation series performed in this study. The first particle of the VSWD always has values of $\sigma_1=1$, $\epsilon_1=1$, $\lambda_1^*=\lambda\sigma_1$, and $\lambda_2^*=\lambda\sigma_1$. The last two columns give T_c^* and ρ_c^* obtained with Eqs. (11) and (12).

Series	σ_2^*	λ_2^*	ϵ_2^*	L^*	L_{vw}^*	T_c^*	ρ_c^*
1	1	1.5	1	1	0.05	1.55	0.299
2	1	1.5	1	1	0.1	1.54	0.300
3	1	1.5	1	1	0.2	1.56	0.298
4	1	1.5	1	0.5	0.05	2.40	0.409
5	1	1.5	1	0.5	0.1	2.37	0.414
6	1	1.5	1	0.5	0.2	2.37	0.421
7	1	1.5	1	0.25	0.05	3.48	0.526
8	1	1.5	1	0.25	0.1	3.42	0.521
9	1	1.5	1	0.25	0.2	3.37	0.525
10	0.5	0.75	1	0.75	0.1	1.62	0.538
11	1	1.5	2	1	0.1	2.29	0.290
12	1	1.5	4	1	0.1	3.40	0.285
13	1	1.5	8	1	0.1	5.30	0.284
14	0.5	0.75	2	0.75	0.1	1.98	0.517
15	0.5	0.75	4	0.75	0.1	2.49	0.500
16	0.5	0.75	8	0.75	0.1	2.18	0.530
17	0.25	0.375	1	0.625	0.1	1.53	0.585
18	0.25	0.375	2	0.625	0.1	1.71	0.568
19	0.25	0.375	4	0.625	0.1	1.96	0.579
20	0.25	0.375	8	0.625	0.1	2.04	0.588

by fitting the calculated density profile to a hyperbolic tangent function,

$$\rho(x)=\tfrac{1}{2}(\rho_L+\rho_V)-\tfrac{1}{2}(\rho_L-\rho_V)\tanh[2(x-x_0)/\delta], \tag{10}$$

where ρ_L and ρ_V are the liquid and vapor densities at the orthobaric curve, respectively, δ is the thickness of the interface, and x_0 is the Gibbs equimolar dividing surface of the interface.

D. Critical temperature and density

The estimation of the critical point was made using the procedure included by Singh *et al.*[36] using a least squares fit of the law of rectilinear diameter and scaling relation,

$$\rho_L-\rho_V=C_1\left(1-\frac{T}{T_c}\right)^{\beta_c}+C_2\left(1-\frac{T}{T_c}\right)^{\beta_c+\Delta}, \tag{11}$$

where C_1 and C_2 are adjusting constants. The critical exponent $\beta_c=0.325$ and $\Delta=0.51$. The critical temperature T_c from Eq. (11) is used in the rectilinear diameter relation to obtain the critical density ρ_c,

$$\frac{\rho_L+\rho_V}{2}=\rho_c+C_3(T-T_c), \tag{12}$$

with C_3 as another constant.

V. DESCRIPTION OF THE SIMULATED SERIES

The reducing parameters are $\sigma_1=1$ for distance and $\epsilon_1=1$ for energy. The size of the vibration well $L_{vw}^*=L_{vw}/\sigma_1$, the elongation $L^*=L/\sigma_1$, the relative size of the two particles $\sigma_2^*=\sigma_2/\sigma_1$, and the relative depth of the interaction well $\epsilon_2^*=\epsilon_2/\epsilon_1$ are used as variables in this study. The ranges of the potential wells are always $\lambda_1^*=\lambda\sigma_1^*$ and $\lambda_2^*=\lambda\sigma_2^*$ using the generic constant $\lambda=1.5$. Figure 1 gives a pictorial description of these variables. The reduced properties are as follows: $T^*=k_BT/\epsilon_1$ for temperature, $\rho^*=\rho\sigma_1^3$ for density, $P^*=P\sigma_1^3/\epsilon_1$, for pressure, and $\gamma^*=\gamma\sigma_1^2/\epsilon_1$ for surface tension.

The series simulated are defined in detail in Table I where the values of the selected variables σ_2^*, λ_2^*, ϵ_2^*, L^*, and L_{vw}^* are given for each series. The critical temperatures T_c^* and densities ρ_c^* obtained from the simulation data are included in the last two columns.

All runs were carried out at the UAM-Iztapalapa cluster. The box was a parallelepiped of 11.9 atomic diameters σ_1 in the y and z directions and six or eight times more in the x direction. The number of particles used in all cases are 5000 (2500 dumbbells) with mass $m=1$, initially positioned in a fcc crystalline array. Blocks of 100×10^6 collisions were performed, with partial results kept every 25×10^6 and accumulation of statistics every 100 000 collisions. An initial equilibration period of an average of 50 blocks were allowed to run. Once the equilibration period was done, the maximum number of blocks for one run was 131, the minimum was 18, and the average was 43 blocks. Surface tension calculation requires long runs as performed in this work because the mean value is obtained from differences of pressure tensor components. When there was need of continuing one run at another set of temperatures, the final configuration of the previous run was selected as the initial configuration.

VI. RESULTS

The results are presented in four main subsections and in Tables II–VI, where simulation results for γ^*, P_V^*, ρ_L^*, and ρ_V^* are given for the 20 series included in Table I. Table III includes the results for the MC runs performed. Section VI A

TABLE II. Simulation results for series 1 and 2. Values for surface tension γ^*, vapor pressure P_V^*, orthobaric liquid ρ_L^*, and vapor ρ_V^* densities are given for each temperature T^*, where simulation values are available. Subindices indicate the error in each data, for example, 0.627_{15} means that the value is 0.627 ± 0.015. Errors are calculated as the mean square deviation of the data divided by the number of blocks performed in each run.

	Series 1			
T^*	γ^*	P_V^*	ρ_L^*	ρ_V^*
1	0.627_{15}	0.0007_0	0.7561_1	$0.001\,77_3$
1.05	0.545_{18}	0.0014_1	0.7408_1	$0.002\,85_4$
1.1	0.488_{11}	0.0023_1	0.7251_1	$0.004\,60_5$
1.15	0.423_{13}	0.0039_1	0.7080_1	$0.007\,52_7$
1.175	0.404_{10}	0.0047_1	0.6993_1	$0.008\,87_8$
1.2	0.375_{13}	0.0057_1	0.6895_1	$0.010\,47_8$
1.225	0.336_{13}	0.0073_1	0.6798_1	$0.014\,00_9$
1.25	0.303_{15}	0.0087_1	0.6707_1	$0.016\,54_9$
1.275	0.290_{11}	0.0105_1	0.6590_1	$0.020\,11_{11}$
1.3	0.253_{11}	0.0122_2	0.6478_1	$0.023\,38_{12}$
1.325	0.244_{13}	0.0148_2	0.6357_1	$0.027\,91_{12}$
1.35	0.183_{11}	0.0177_3	0.6235_1	$0.035\,34_{16}$
1.375	0.162_8	0.0205_2	0.6086_1	$0.040\,88_{15}$
1.425	0.108_{10}	0.0276_4	0.5762_1	$0.058\,06_{20}$
1.475	0.082_8	0.0365_4	0.5348_1	$0.084\,11_{25}$
		Series 2		
1	0.615_9	0.0007_0	0.7566_2	$0.001\,49_3$
1.05	0.551_8	0.0014_0	0.7419_1	$0.002\,73_6$
1.1	0.485_7	0.0023_0	0.7261_1	$0.004\,58_8$
1.15	0.428_7	0.0038_0	0.7114_2	$0.008\,03_{14}$
1.175	0.410_{11}	0.0049_1	0.6992_1	$0.009\,64_7$
1.2	0.356_6	0.0058_1	0.6898_1	$0.010\,14_{17}$
1.225	0.346_{11}	0.0072_1	0.6808_1	$0.013\,14_9$
1.25	0.307_6	0.0086_1	0.6710_1	$0.016\,57_{31}$
1.275	0.281_{15}	0.0102_1	0.6595_1	$0.019\,19_{11}$
1.3	0.267_7	0.0124_1	0.6478_1	$0.024\,58_{39}$
1.325	0.213_9	0.0146_2	0.6375_1	$0.027\,42_{13}$
1.35	0.200_5	0.0171_1	0.6299_1	$0.030\,43_{54}$
1.375	0.164_{11}	0.0204_2	0.6090_1	$0.040\,48_{15}$
1.425	0.112_7	0.0273_3	0.5777_1	$0.053\,89_{18}$
1.475	0.064_8	0.0364_4	0.5311_1	$0.088\,64_{26}$

TABLE III. Simulation results for series 3–6. See the caption of Table II. This table includes, at the bottom, the results from the MC runs performed.

	Series 3			
T^*	γ^*	P_V^*	ρ_L^*	ρ_V^*
1	0.621_7	0.0007_0	0.7600_1	$0.001\,48_4$
1.05	0.556_7	0.0014_0	0.7440_1	$0.003\,27_8$
1.1	0.494_7	0.0023_0	0.7296_1	$0.005\,15_{11}$
1.15	0.435_8	0.0037_1	0.7101_1	$0.006\,94_{15}$
1.175	0.401_{12}	0.0047_1	0.7014_1	$0.008\,54_7$
1.2	0.357_7	0.0057_1	0.6913_1	$0.010\,11_{15}$
1.225	0.341_{12}	0.0072_1	0.6820_1	$0.013\,14_9$
1.25	0.318_6	0.0086_1	0.6719_1	$0.014\,61_{25}$
1.275	0.301_8	0.0106_2	0.6614_1	$0.020\,19_{11}$
1.3	0.253_6	0.0121_1	0.6484_1	$0.025\,65_{42}$
1.325	0.232_9	0.0149_1	0.6371_1	$0.028\,04_{13}$
1.35	0.186_6	0.0173_1	0.6229_1	$0.034\,43_{67}$
1.375	0.173_8	0.0207_2	0.6095_1	$0.041\,65_{15}$
1.425	0.108_9	0.0273_3	0.5778_1	$0.056\,52_{17}$
1.475	0.059_7	0.0368_3	0.5367_1	$0.082\,33_{20}$
		Series 4		
1.4	1.354_{23}	0.0006_1	1.0984_3	$0.000\,78_2$
1.6	1.051_{18}	0.0037_1	1.0379_2	$0.004\,12_9$
1.8	0.744_{20}	0.0123_2	0.9708_2	$0.014\,06_{28}$
2	0.416_{13}	0.0317_3	0.8880_2	$0.041\,23_{70}$
2.2	0.177_{12}	0.0689_5	0.7919_1	$0.083\,63_{139}$
		Series 5		
1.4	1.351_{23}	0.0006_0	1.1094_2	$0.002\,27_2$
1.6	1.050_{22}	0.0035_1	1.0442_3	$0.004\,87_9$
1.8	0.751_{18}	0.0123_1	0.9763_2	$0.015\,19_{27}$
2	0.439_{17}	0.0317_2	0.8957_2	$0.035\,50_{61}$
2.2	0.180_{10}	0.0698_5	0.7856_2	$0.101\,20_{162}$
		Series 6		
1.4	1.523_{32}	0.0004_1	1.1478_8	$0.000\,83_1$
1.6	1.093_{22}	0.0031_1	1.0794_5	$0.004\,28_4$
1.3	0.405_7	0.0199_2	1.2069_1	$0.033\,40_{29}$
1.325	0.400_7	0.0234_2	1.1915_1	$0.044\,13_{43}$
1.8	0.796_{15}	0.0117_2	1.0062_5	$0.013\,92_6$
2	0.484_{13}	0.0309_3	0.9198_4	$0.038\,23_6$
2.2	0.183_{11}	0.0686_5	0.7996_4	$0.098\,49_9$
		MC		
1.20	0.35_2	0.0100	0.699	0.0112
1.25	0.27_2	0.0074	0.668	0.0106
1.30	0.26_2	0.0083	0.644	0.0222
1.35	0.20_2	0.0157	0.620	0.0350
1.40	0.13_3	0.0207	0.588	0.0492
1.45	0.08_3	0.0309	0.550	0.0730
1.50	0.03_3	0.0403	0.480	0.1210

gives the analysis of the effect of the size of the vibrating well L_{vw}^* for various elongations L^* of homonuclear dumbbells. Section VI B analyzes the effect of the elongation L^* for the case for overlapping homonuclear dumbbells. Section VI C discusses the effect of decreasing the size of one of the particles σ_2^* for tangent heteronuclear dumbbells. Section VI D includes the results of the effect of increasing the well depth ϵ_2^* for homonuclear and heteronuclear dumbbells.

A. Effect of L_{vw}^*: The size of the vibrating well

The effect of L_{vw}^* is quite small, and in order to give a much accurate picture of the comparison of the results for the orthobaric densities with previously reported data, a reduced portion of series 2 is given in Fig. 2, which presents data obtained for homonuclear VSWD with $L^*=1$ and $L_{vw}^*=0.05$, 0.1, and 0.2. These results are compared with MC results by Kim *et al.*,[18] MC simulations by Escobedo and de Pablo[16] and Yethiraj and Hall[13] and DMD results by Hu *et al.*[10] The agreement among the data is fair, and the scatter is around the points obtained in this work. However, the best agreement is with the MC data of Kim *et al.*[18] The DMD results by Hu *et al.*[14] are high with respect to the rest of the data, probably due to the fact that the reduced elongation of their dumbbells L^* is not 1 but 0.985, producing a smaller molecule and hence a higher critical point. In general, this variable has a small impact on the properties selected in comparison to the effects of the rest of the variables analyzed. Since the data are at the same temperature, a direct comparison of the results was performed. Data with $L_{vw}^*=0.1$ were

TABLE IV. Simulation results for series 7–11. See the caption of Table II.

T^*	γ^*	P_V^*	ρ_L^*	ρ_V^*
		Series 7		
2.5	1.366_{22}	0.0166_{2}	1.2036_{19}	$0.014\,65_{11}$
2.61	1.202_{22}	0.0240_{2}	1.1772_{18}	$0.017\,75_{14}$
2.72	0.984_{19}	0.0352_{2}	1.1536_{13}	$0.022\,77_{9}$
2.83	0.848_{18}	0.0484_{3}	1.1082_{19}	$0.042\,08_{16}$
2.94	0.645_{17}	0.0666_{4}	1.0924_{10}	$0.069\,08_{15}$
3.05	0.475_{14}	0.0879_{4}	1.0370_{11}	$0.075\,12_{27}$
3.16	0.337_{14}	0.1144_{5}	0.9985_{10}	$0.108\,11_{35}$
3.27	0.205_{14}	0.1480_{6}	0.9070_{11}	$0.171\,00_{37}$
		Series 8		
2.5	1.395_{22}	0.0172_{2}	1.2024_{16}	$0.017\,63_{11}$
2.61	1.193_{20}	0.0253_{2}	1.1757_{15}	$0.020\,45_{10}$
2.72	0.967_{14}	0.0355_{2}	1.1422_{13}	$0.028\,24_{18}$
2.83	0.807_{15}	0.0501_{3}	1.1120_{12}	$0.044\,22_{16}$
2.94	0.618_{16}	0.0679_{4}	1.0712_{12}	$0.057\,88_{15}$
3.05	0.461_{15}	0.0904_{4}	1.0319_{12}	$0.074\,60_{19}$
3.16	0.348_{12}	0.1188_{4}	0.9876_{12}	$0.102\,19_{34}$
3.27	0.184_{9}	0.1538_{6}	0.9083_{10}	$0.173\,04_{24}$
		Series 9		
2.5	1.334_{18}	0.0188_{1}	1.2083_{13}	$0.018\,62_{14}$
2.61	1.151_{21}	0.0275_{2}	1.1786_{18}	$0.023\,28_{11}$
2.72	0.979_{15}	0.0394_{3}	1.1453_{11}	$0.033\,81_{15}$
2.83	0.747_{12}	0.0552_{4}	1.1087_{12}	$0.048\,33_{15}$
2.94	0.581_{14}	0.0754_{3}	1.0754_{12}	$0.059\,46_{15}$
3.05	0.422_{13}	0.1000_{5}	1.0246_{14}	$0.101\,00_{31}$
3.16	0.275_{11}	0.1312_{5}	0.9645_{11}	$0.117\,82_{35}$
3.27	0.135_{8}	0.1692_{5}	0.8886_{6}	$0.185\,18_{39}$
		Series 10		
1	0.907_{9}	0.0014_{0}	1.3995_{2}	$0.003\,15_{4}$
1.05	0.817_{11}	0.0025_{1}	1.3706_{1}	$0.004\,00_{6}$
1.1	0.744_{9}	0.0041_{1}	1.3421_{2}	$0.006\,12_{7}$
1.15	0.668_{10}	0.0064_{1}	1.3130_{2}	$0.014\,52_{16}$
1.2	0.584_{8}	0.0097_{1}	1.2797_{2}	$0.017\,53_{17}$
1.225	0.543_{8}	0.0118_{1}	1.2639_{1}	$0.022\,04_{20}$
1.25	0.492_{7}	0.0141_{1}	1.2459_{1}	$0.022\,97_{23}$
1.275	0.458_{7}	0.0168_{1}	1.2304_{1}	$0.024\,93_{21}$
1.3	0.405_{7}	0.0199_{2}	1.2069_{1}	$0.033\,40_{29}$
1.325	0.400_{7}	0.0234_{2}	1.1915_{1}	$0.044\,13_{43}$
1.35	0.337_{8}	0.0273_{1}	1.1697_{1}	$0.044\,59_{41}$
1.375	0.303_{6}	0.0318_{2}	1.1495_{2}	$0.053\,73_{50}$
1.425	0.224_{7}	0.0426_{3}	1.1101_{1}	$0.076\,37_{62}$
1.475	0.169_{7}	0.0557_{3}	1.0456_{1}	$0.099\,42_{85}$
1.525	0.106_{11}	0.0722_{3}	0.9850_{1}	$0.151\,37_{128}$
1.575	0.033_{3}	0.0933_{3}	0.8745_{2}	$0.212\,17_{179}$
		Series 11		
1.4	0.880_{15}	0.0006_{0}	0.7658_{1}	$0.001\,44_{3}$
1.5	0.788_{16}	0.0015_{1}	0.7478_{1}	$0.002\,96_{5}$
1.6	0.655_{12}	0.0032_{1}	0.7227_{1}	$0.003\,71_{6}$
1.7	0.537_{14}	0.0064_{1}	0.6988_{1}	$0.008\,73_{10}$
1.8	0.438_{13}	0.0110_{1}	0.6700_{1}	$0.013\,96_{11}$
1.9	0.324_{11}	0.0176_{1}	0.6456_{1}	$0.021\,30_{22}$
2	0.223_{9}	0.0278_{2}	0.6093_{1}	$0.035\,21_{33}$
2.1	0.133_{9}	0.0430_{2}	0.5568_{1}	$0.051\,35_{43}$

TABLE V. Simulation results for series 12–15. See the caption of Table II.

T^*	γ^*	P_V^*	ρ_L^*	ρ_V^*
		Series 12		
2.2	1.007_{28}	0.0011_{1}	0.7544_{2}	$0.000\,91_{2}$
2.3	0.919_{18}	0.0018_{1}	0.7388_{1}	$0.002\,84_{2}$
2.4	0.843_{34}	0.0031_{1}	0.7266_{1}	$0.002\,21_{3}$
2.5	0.752_{24}	0.0051_{1}	0.7107_{1}	$0.004\,89_{4}$
2.6	0.660_{24}	0.0075_{1}	0.6929_{1}	$0.006\,11_{6}$
2.7	0.578_{17}	0.0108_{2}	0.6729_{1}	$0.009\,20_{5}$
2.8	0.501_{26}	0.0159_{2}	0.6571_{1}	$0.014\,93_{10}$
2.9	0.383_{23}	0.0221_{3}	0.6321_{1}	$0.016\,96_{7}$
3	0.300_{15}	0.0301_{2}	0.6077_{2}	$0.025\,78_{5}$
3.1	0.235_{15}	0.0397_{3}	0.5757_{2}	$0.035\,39_{4}$
3.2	0.174_{13}	0.0530_{4}	0.5383_{1}	$0.052\,93_{4}$
		Series 13		
2.9	1.163_{84}	-0.0001_{1}	0.7972_{3}	$0.000\,00_{0}$
3.1	0.953_{66}	-0.0001_{1}	0.7921_{4}	$0.000\,02_{0}$
3.3	0.987_{47}	0.0000_{1}	0.7730_{3}	$0.000\,10_{0}$
3.5	0.838_{40}	0.0002_{1}	0.7555_{2}	$0.000\,24_{0}$
3.7	0.872_{40}	0.0008_{1}	0.7382_{2}	$0.000\,53_{0}$
3.9	0.724_{32}	0.0018_{1}	0.7176_{2}	$0.001\,00_{1}$
4.1	0.684_{33}	0.0036_{1}	0.6985_{2}	$0.001\,99_{1}$
4.3	0.596_{30}	0.0067_{2}	0.6762_{2}	$0.003\,94_{1}$
4.5	0.470_{27}	0.0110_{2}	0.6503_{2}	$0.005\,56_{2}$
		Series 14		
1.4	0.685_{13}	0.0062_{1}	1.3213_{2}	$0.010\,89_{11}$
1.5	0.561_{13}	0.0126_{1}	1.2623_{2}	$0.016\,13_{12}$
1.6	0.409_{8}	0.0228_{2}	1.2069_{1}	$0.031\,82_{26}$
1.7	0.279_{8}	0.0387_{2}	1.1261_{1}	$0.046\,88_{43}$
1.8	0.152_{7}	0.0630_{3}	1.0144_{3}	$0.124\,33_{100}$
		Series 15		
1.6	0.537_{23}	0.0008_{1}	1.3383_{7}	$0.000\,58_{1}$
1.7	0.469_{21}	0.0019_{1}	1.3072_{7}	$0.001\,26_{2}$
1.8	0.400_{21}	0.0041_{1}	1.2669_{5}	$0.005\,74_{6}$
1.9	0.369_{19}	0.0080_{1}	1.2286_{3}	$0.009\,22_{12}$
2	0.295_{13}	0.0139_{1}	1.1814_{4}	$0.016\,59_{12}$
2.1	0.254_{10}	0.0235_{2}	1.1205_{3}	$0.028\,30_{27}$
2.2	0.171_{11}	0.0380_{3}	1.0600_{8}	$0.045\,00_{9}$
2.3	0.078_{11}	0.0575_{3}	0.9411_{8}	$0.091\,44_{16}$

selected as the base results and the other two were compared to these. Table VII gives the average percentage deviations of these comparisons. For $L^*=1$, averages are within simulation errors for all the properties ($<0.6\%$) except for ρ_V^*, which is ($\sim 3\%$). As the particles in the molecule get closer together the average percentage deviations increase for all the properties, as can be seen in Fig. 2 and Table VII. These might be due to the fact that increments in percentage variations in molecular volume follow a similar tendency as the increments for the relative percentage deviations, as shown in the last three columns of Table VII. Careful analysis of the distribution of the percentage deviations indicate that there is not a tendency to any particular bias due to temperature.

Another way to analyze these results is through the critical properties. The effect of L_{vw}^* on T_c^* and ρ_c^* is quite minor as well. For values of L_{vw}^* going from 0.05, to 0.1, and to 0.2, T_c^* increases from $1.55\pm0.4\%$, to $2.38\pm0.7\%$, and to $3.42\pm1.6\%$ for $L^*=1$, 0.5, and 0.25, respectively. For the same values of L_{vw}^* and L^*, the critical density ρ_c^* increases from $0.3\pm0.3\%$, to $0.41\pm1.5\%$, and to $0.5\pm0.5\%$. The variations in these calculated values are, in all cases, less

TABLE VI. Simulation results for series 16–20. See the caption of Table II.

	Series 16			
T^*	γ^*	P_V^*	ρ_L^*	ρ_V^*
1.9	0.297_{26}	0.0001_0	1.2455_{10}	$0.003\,16_4$
2	0.104_{22}	0.0007_1	1.2025_7	$0.032\,25_{29}$
2.1	0.039_{12}	0.0020_1	1.0495_8	$0.049\,39_{51}$
	Series 17			
1	0.790_{10}	0.0030_1	1.5456_6	$0.006\,28_3$
1.06	0.700_{11}	0.0056_1	1.5032_5	$0.011\,14_4$
1.12	0.590_{11}	0.0093_1	1.4602_5	$0.018\,00_7$
1.18	0.512_{10}	0.0149_1	1.4142_4	$0.027\,84_7$
1.24	0.417_7	0.0226_2	1.3629_5	$0.042\,93_8$
1.3	0.326_6	0.0326_2	1.3106_5	$0.060\,12_{10}$
1.36	0.237_6	0.0466_2	1.2454_5	$0.091\,68_7$
1.42	0.146_4	0.0636_2	1.1663_5	$0.128\,66_{16}$
1.46	0.096_3	0.0777_2	1.0135_{112}	$0.166\,31_9$
1.5	0.046_3	0.0944_2	0.9241_{36}	$0.226\,99_{13}$
	Series 18			
1	0.877_{15}	0.0004_0	1.6573_{101}	$0.001\,42_2$
1.1	0.775_{10}	0.0018_0	1.6060_{26}	$0.003\,75_3$
1.2	0.662_9	0.0050_1	1.5384_{28}	$0.007\,61_3$
1.3	0.549_7	0.0116_1	1.4649_{17}	$0.019\,46_6$
1.4	0.409_6	0.0228_1	1.3801_6	$0.042\,90_7$
1.5	0.281_5	0.0410_2	1.2886_8	$0.069\,62_{10}$
1.6	0.143_4	0.0678_2	1.1786_6	$0.124\,04_{15}$
1.7	0.019_3	0.1082_2	0.7145_4	$0.286\,78_{21}$
	Series 19			
1.24	0.611_{25}	0.0000_0	1.5175_{53}	$0.001\,67_2$
1.36	0.485_{23}	0.0006_0	1.4536_{45}	$0.005\,41_4$
1.48	0.341_{16}	0.0026_1	1.3614_{37}	$0.019\,59_{20}$
1.6	0.280_{12}	0.0083_1	1.2572_{17}	$0.046\,85_{18}$
1.72	0.180_8	0.0207_1	1.1381_{12}	$0.105\,05_{29}$
1.84	0.083_6	0.0445_2	1.0000_0	$0.180\,00_0$
	Series 20			
1.3	0.480_{46}	-0.0001_0	1.7243_{154}	$0.000\,00_0$
1.45	0.386_{28}	0.0002_0	1.5783_{62}	$0.000\,51_1$
1.6	0.290_{21}	0.0014_1	1.4486_{47}	$0.014\,37_9$
1.75	0.161_{17}	0.0047_1	1.3277_{26}	$0.040\,18_{18}$
1.9	0.061_8	0.0150_2	1.1500_{19}	$0.150\,00_{55}$

than 1.6%. This could be important because wider vibrating wells promote much faster simulations since tightly constrained vibrating wells are rapidly colliding. Faster simulations can probe longer time scales and mesoscale behavior. There may be theoretical implications also since such behavior would indicate the feasibility of simplifying assumptions.

B. Effect of L^*: Elongation

The elongation has a much larger effect on the properties observed. In terms of the critical temperature, the average values goes from $T_c=3.42$, to 2.38, and to 1.55 for $L_*=0.25$, 0.5, and 1, respectively. This means that the T_c's have a maximum decrease of 45%, while the critical densities present average values that go from $\rho_c^*=0.52$, to 0.41, and to 0.3 with a maximum decrease of 57%. Figure 3 includes series 1–9 and gives orthobaric densities ρ_L^* and ρ_V^* (top), surface tension γ^* (middle), and vapor pressure P_v (bottom) for elongations $L^*=1$, 0.5, and 0.25 and vibrating well lengths $L_{\mathrm{vw}}^*=0.05$, 0.1, and 0.2. Elongation L^* has a large effect on these properties, increasing considerably the critical temperature and producing a small increase in critical density with decreasing elongation. Orthobaric densities are compared with the values reported by Hu *et al.*[14] for $L^*=0.97$, 0.6, and 0.4. Even though elongations do not match, the general trend of the curves and their position are correct. Surface tension is included in the middle panel of the plot. The slope of γ^* versus T^* increases slightly with decreasing L^* and the value of $L_{vw}^*=0.2$ has only a limited effect for values of $L^*=0.5$ and 0.25. In the first case, γ^* increases at low temperatures and decreases at high temperatures for $L^*=0.25$. This same middle figure reports the values for the surface tension γ^* obtained with MC (included at the bottom part of Table VII) using equations given in Sec. IV B. At the bottom panel, the results for vapor pressure P_V^* are given for the same three series and compared with the reported DMD values by Hu *et al.*[14] for $L^*=1$. The agreement of these data is fair.

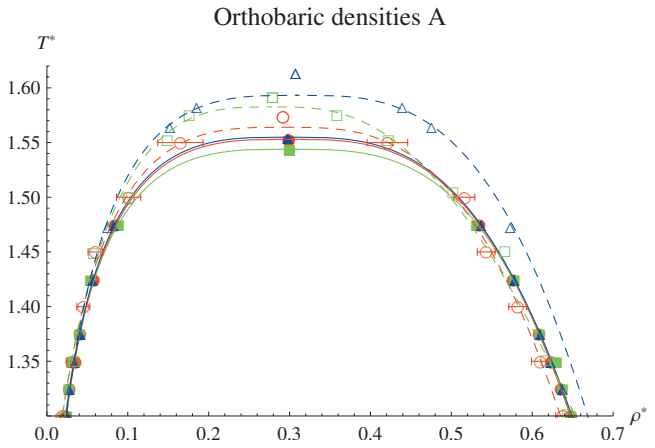

FIG. 2. Effect of L_{vw}^* on orthobaric densities. The figure plots the orthobaric densities of homonuclear vibrating dumbbells (series 1–3). Full circles, squares, and triangles are the results for VSWD with L_{vw}^* values of 0.05, 0.1, and 0.2, respectively. Open circles are SWD MC values by Kim *et al.* (Ref. 18), open squares are SWD MC data by Escobedo *et al.* (Ref. 16), and Yethiraj *et al.* (Ref. 13), and open triangles are VSWD DMD results by Hu *et al.* (Ref. 14) VSWD and SWD are different systems. The main discrepancy of these two systems is the intramolecular potential. While the SWD is bonded at a fix distance, the VSWD is bonded by a SW potential of range $L_{\mathrm{vw}}{}^*$ with infinite walls.

C. Effect of σ_2^*: Size of the second particle

The particle size has a large effect on both critical temperature and density. Care must be exercised in the analysis of these data because the variation in σ_2^* is accompanied by a change in the range of the potential well given by $\lambda_2^*=\lambda\sigma_2^*$, with $\lambda=1.5$. Tangent VSWDs with second particle sizes $\sigma_2^*=0.25$, 0.5, and 1 were simulated to evaluate this effect and four different values of $\epsilon_2^*=1$, 2, 4, and 8 are included. Average values of critical density decrease monotonically for the σ_2^*'s considered as: $\rho_c^*=0.58\pm1.5\%$, $0.52\pm3.2\%$, and $0.29\pm2.5\%$, respectively. Each one of the ρ_c^* curves for the ϵ_2^*'s mentioned above behave in the same manner. The maximum deviation of the critical density for

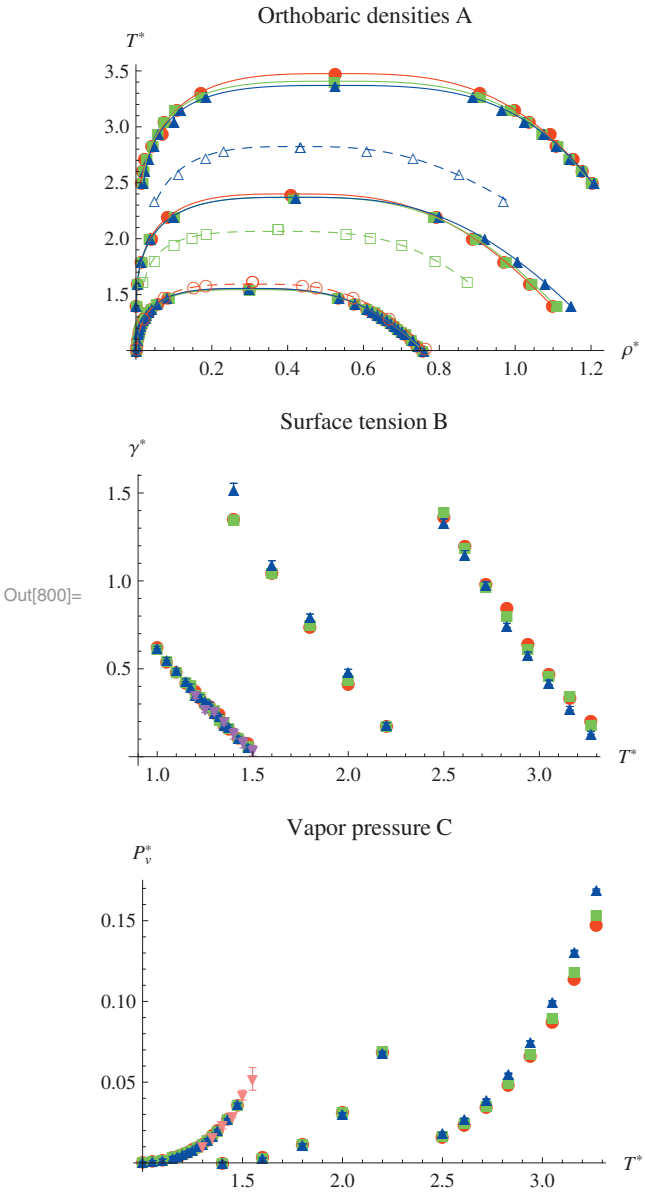

FIG. 3. Effect of L^*_{vw} on orthobaric densities (top), surface tension (middle), and vapor pressure (bottom) which correspond to tangent and overlapping homonuclear VSWD having $L^*=1$, 0.5, 0.25 (series 1–9). The top panel includes the orthobaric densities with full circles, squares, and triangles from results of this work for VSWD with $L^*_{vw}=0.05$, 0.1, 0.2, respectively. From the bottom up curves represent series with elongation $L^*=1$, 0.5, 0.25. Open circles, squares, and triangles are the values reported by Kim *et al.* (Ref. 18) for $L^*=0.97$, 0.6, 0.4, and $L^*_{vw}=0.03$, 0.1, 0.1. Surface tension data are depicted at the bottom panel with decreasing values of $L^*=1$, 0.5, 0.25 going from left to right.

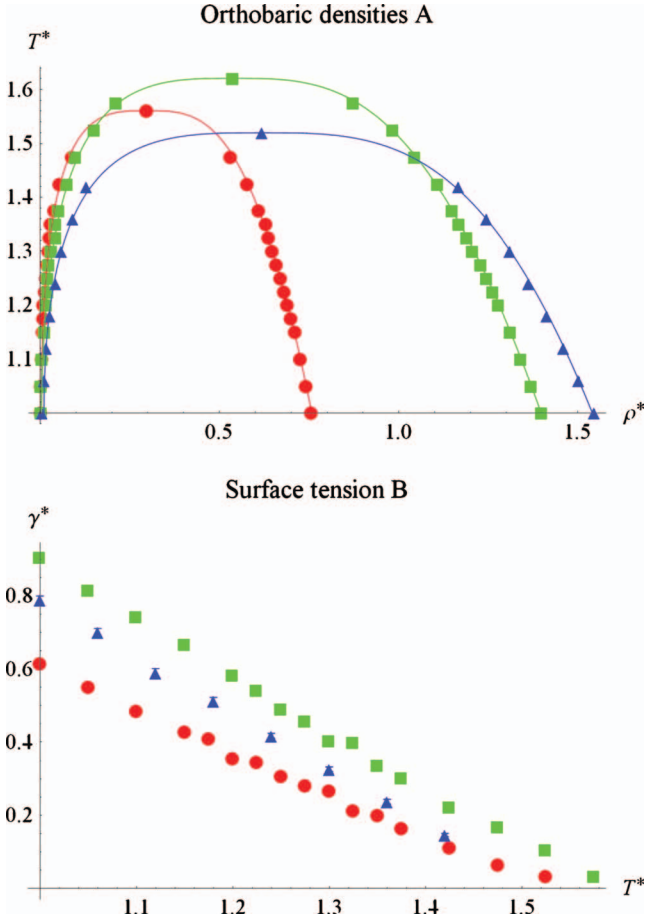

FIG. 4. Orthobaric densities (top) and surface tension (bottom) for series 2, 10, and 17 corresponding to tangent homonuclear and heteronuclear VSWDs with sizes of the second particle $\sigma^*_2=1$ (circles), 0.5 (squares), and 0.25 (triangles).

all the ϵ^*_2's is 50%. Variations in the critical temperature T^*_c have different behaviors for each ϵ^*_2, when the series of σ^*_2's are considered. For $\epsilon^*_2=1$, the values of $T^*_c=1.53$, 1.62, and 1.54 present a maximum at $\sigma^*_2=0.5$. For $\epsilon^*_2=2$ and 4, the values of T^*_c increase monotonically. For $\epsilon^*_2=8$, the values of $T^*_c=2.04$, 2.18, and 5.3 are flat at the beginning and then exhibit a large increase at $\sigma^*_2=1$. Figure 4 presents the results obtained for series 2, 10, and 17 and the data are given in Tables II, IV, and VI. This group of series presents a maximum in T^*_c at $\sigma^*_2=0.5$ for $\epsilon^*_2=1$. The upper panel presents the orthobaric densities and the lower one gives the surface tension. In this figure the most striking effect is that the critical temperature increases at first from $\sigma^*_2=1$ to $\sigma^*_2=0.5$ and then it decreases for $\sigma^*_2=0.25$. This initial increase might be do to the fact that two opposing effects are acting in this case. It is known that a decrease in λ produces a decrease in the critical temperature[37,38] and that a decrease in molecular volume σ^*_2 produces an increase in critical temperature for the same well size and depth (see Fig. 3). It must be remembered that a change in σ^*_2 means that λ^*_2 also changes. Surface tensions show the typical shape with increasing values when going from $\sigma^*_2=1$ to $\sigma^*_2=0.5$ and decreasing later for $\sigma^*_2=0.25$.

D. Effect of ϵ^*_2: SW depth of the second particle

Series (2, 11, 12, 13), (10, 14, 15, 16), and (17, 18, 19, 20) are used to study the effect of the SW depth of the second particle ϵ^*_2. These three groups are for tangent VSWD with ϵ^*_2's=1, 2, 4, and 8. Each group corresponds to values of $\sigma^*_2=1$, 0.5, and 0.25, respectively ($\lambda^*_2=1.5\sigma^*_2$). The effect of ϵ^*_2 on the critical density is very small. Average values of critical density for each σ^*_2 considered are $\rho^*_c=0.58\pm1.5\%$, $0.52\pm3.2\%$, and $0.29\pm2.5\%$, respectively. Variations in the critical temperature T^*_c are larger and with different behaviors for each σ^*_2 when the series of ϵ^*_2 are considered. For $\sigma^*_2=1$, the values of $T^*_c=1.54$, 2.29, 3.4, and 5.3 increase

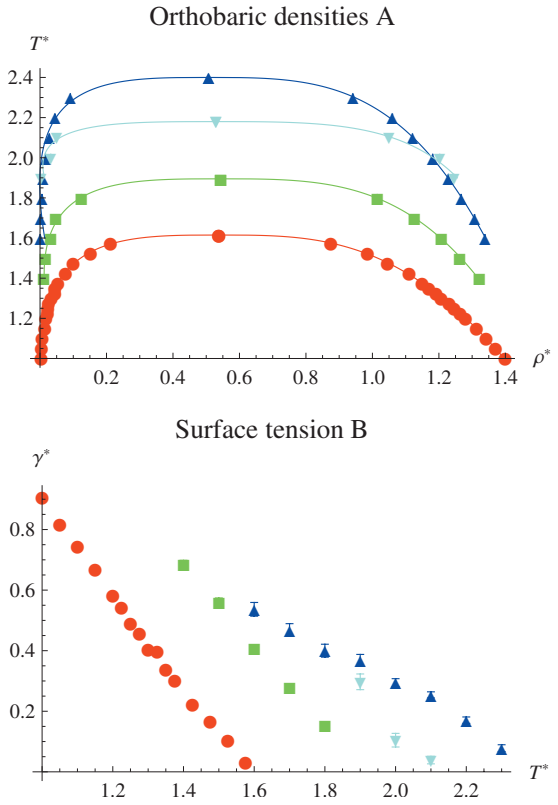

FIG. 5. Orthobaric densities (top) and surface tension (bottom) for series 10, 14, 15, and 16 corresponding to heteronuclear tangent VSWD with $\sigma_2^*=0.5$. Circles, squares, triangles, and inverted triangles are for $\epsilon_2^*=1$, 2, 4, and 8, respectively.

monotonically with a total increase of 3.4 times the initial value. For $\sigma_2^*=0.5$, the values of $T_c^*=1.62$, 1.98, 2.49, and 2.18 present a maximum at $\epsilon_2^*=4$ with a maximum increase, up to the maximum, of 1.54 times the initial value. For $\sigma_2^*=0.25$, the values of $T_c^*=1.53$, 1.71, 1.96, and 2.04 increase monotonically but it flattens at $\epsilon_2^*=4$, with a total increase of 1.3 times the initial value, hinting that for larger values of $\epsilon_2^*=8$, it might show a maximum value as in the case of $\sigma_2^*=0.5$. The upper panel of Fig. 5 gives orthobaric density results for heteronuclear tangent VSWD with $\sigma_2^*=0.5$, which is the most interesting case due to the existence of a maximum of the critical temperature. The values of the critical density $\rho_c^*=0.52\%-1.5\%$ are very similar, but the values of the critical temperature present a maximum, increasing systematically, at first, going from $T_c^*=1.62$, 1.98, and 2.49 for $\epsilon_2^*=1$, 2, and 4, respectively, and then decreases to $T_c^*=2.18$ for $\epsilon_2^*=8$.

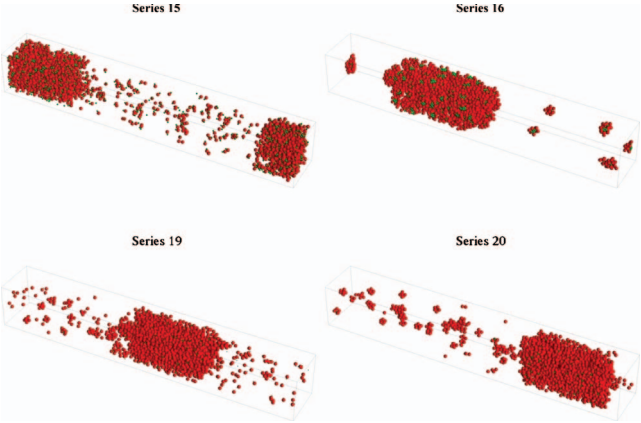

FIG. 6. The top panels show a typical snapshot configuration of series 15 and 16. Both have $\sigma_2^*=0.5$ and $\epsilon_2^*=4$ and 8, respectively, with T^* as near the near the critical point as possible. The bottom panels show a typical snapshot configuration of series 19 and 20. Both have $\sigma_2^*=0.25$ and $\epsilon_2^*=4$ and 8, respectively, with T^* as near the near the critical point as possible. Aggregates of molecules are seen in both phases of all pictures. The nature (size and shape) of them varies substantially for the top figures, in contrast to the bottom ones, which have very similar aggregates, only fewer in the left panel.

It is striking that the critical temperature is lower than that for the case of $\epsilon_2^*=4$ and the solid phase presents itself at a much higher temperature. This might be due to the strong association presented by this system. Figure 6 shows four configuration snapshots corresponding to series 15, 16, 19, and 20 as close to the critical point as possible. Series 15 and 16 are for heteronuclear VSWD with $\sigma_2^*=0.5$ and $\epsilon_2^*=4$ and 8, respectively. Series 19 and 20 are for heteronuclear VSWD with $\sigma_2^*=0.25$ and $\epsilon_2^*=4$ and 8, respectively. The nature of the association is qualitatively different. While series 15 ($\epsilon_2^*=4$) presents practically no association, series 16 ($\epsilon_2^*=4$) shows molecular aggregates that are evident even in the vapor phase, with the smaller more attractive particles, gathered in the inner part of the aggregate. Within the liquid phase one can appreciate the same aggregates but they seem to be larger and interconnected. In the case of Series 19 and 20 the nature of the association is very similar for both values of ϵ_2^*'s, with a larger concentration of aggregates for the larger value of $\epsilon_2^*=8$. By direct inspection of the configuration snapshots it seems that, in this case of smaller molecules ($\sigma_2^*=0.25$), the attraction saturates and the aggregates are not able to grow larger than 5 or 6 dumbbells, while the larger molecules ($\sigma_2^*=0.5$) have sizes that go from 8 up to around 30 dumbbells. Series for $\sigma_2^*=1$ and 0.25 present orthobaric

TABLE VII. Analysis of the effect of L_{vw}^* for homonuclear VSWD with different elongations L^*, expressed as the absolute value of the average percentage deviations form the base case of $L_{vw}^*=0.1$. Values at the extreme right of the table are the percentage variations of the volume of the VSWD for $L_{vw}^*=0.05$, 0.1, and 0.2 for elongations $L^*=1$, 0.5 and 0.25. The increase in percentage variations with both L^* and L_{vw}^* follow similar percentage increases in the volume of the molecule.

	γ^*	P_V^*	ρ_L^*	ρ_V^*	γ^*	P_V^*	ρ_L^*	ρ_V^*	L_{vw}^*	L_{vw}^*	L_{vw}^*
L^*/L_{vw}^*	0.05				0.2				0.05	0.1	0.2
1	0.1	−0.5	0.2	−3.2	0.6	−0.2	0.1	1.1	0.01	0.05	0.18
0.5	1.5	−0.9	0.4	6.0	5.1	−5.6	2.7	−4.6	1.7	3.3	6.7
0.25	−2.6	3.1	−1.2	6.2	−11.7	9.2	−0.5	11.4	2.8	5.6	11.1

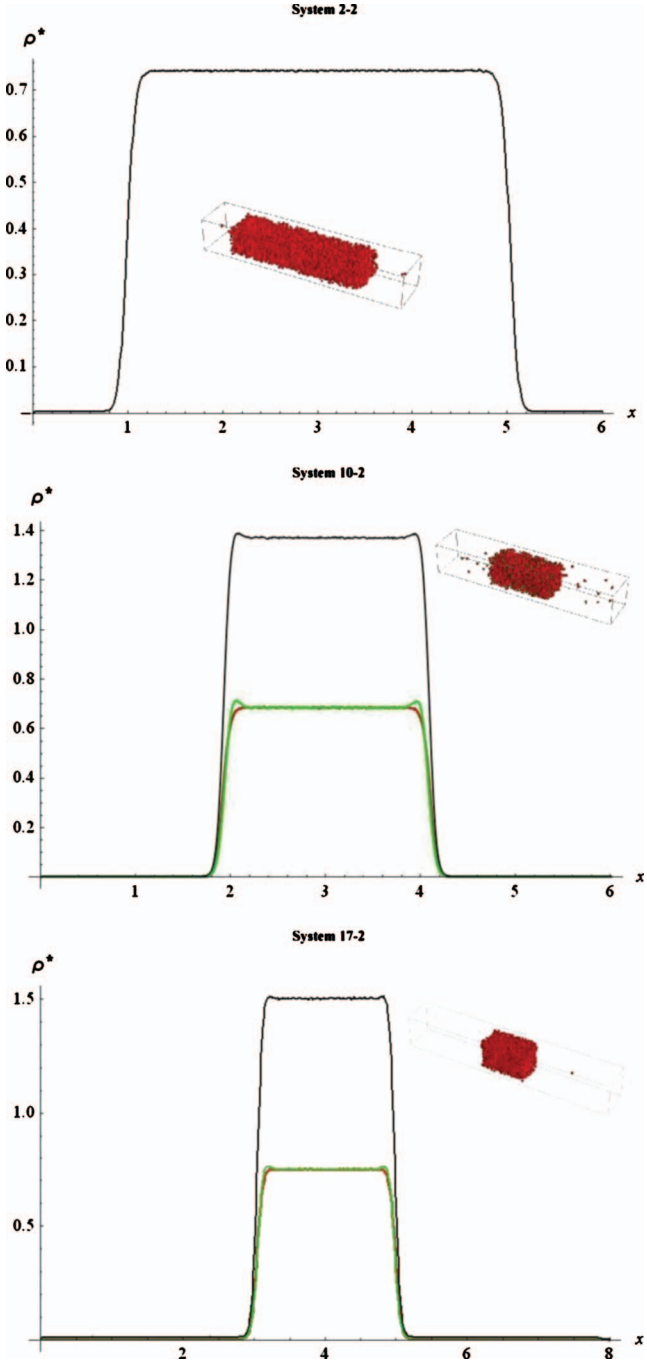

FIG. 7. Density profiles for homonuclear dumbbells series 2 with $\sigma_2^*=1$ at $T^*=1.05$, heteronuclear dumbbells of series 10 with $\sigma_2^*=0.5$ at $T^*=1.05$, and heteronuclear dumbbells of series 17 with $\sigma_2^*=0.25$ at $T^*=1.06$, from top to bottom. The three series have $\epsilon_2^*=1$. As an inset, every profile has a snapshot of one configuration taken during the run.

curves very similar to the ones shown in Fig. 5, except that all of the critical temperatures grow monotonically with growing ϵ_2^*.

For homonuclear tangent VSWD, the results for surface tension γ^* present increasing values of γ^* with similar slopes for $\epsilon_2^*=1$, 2, and 4. For $\epsilon_2^*=8$, γ^* increases also, but the slope with respect to temperature diminishes. Heteronuclear tangent VSWDs with $\sigma_2^*=0.5$, shown of the bottom panel of Fig. 5, present the same general behavior just described for the homonuclear tangent case for $\epsilon_2^*=1$ and 2. For $\epsilon_2^*=4$, γ^* values are not as high than the homonuclear case and at lower temperatures, they have similar values with a diminishing slope. For $\epsilon^*=8$, γ^* values are smaller than those of the previous case described ($\epsilon^*=4$) and the curve of γ^* versus temperature presents a nonlinear tendency with larger error bars even for longer runs. Heteronuclear tangent VSWD with $\sigma_2^*=0.25$ shows very similar results as for the case of $\sigma_2^*=0.5$ (Fig. 5) except that the last two curves, corresponding to $\epsilon^*=4$ and 8, lie on top of each other.

In terms of the density profiles, Fig. 7 presents some typical examples for series 2, 10, and 17 where a well developed planar interface is formed. The homonuclear dumbbell (series 2) presents a usual profile without any specific features. Series 10 and 17 have a little absorbtion of type 2 atoms in the interphase, larger for $\sigma_2^*=0.5$ than for 0.25. Other profiles present similar features at low temperatures. The aggregates mention above has some effect on the profile and perhaps are responsible for the adsorption. As an inset, every profile has a snapshot of one configuration taken during the run.

VII. CONCLUDING REMARKS

A comprehensive study of the influence of four variables on surface tension γ^* and orthobaric densities ρ_L^* and ρ_V^* is presented. The four variables are the size of the vibration well L_{vw}^*, the elongation L^* (also known as the separation of the centers of the particles composing the VSWD) the relative size of the second particle σ_2^*, and the relative depth ϵ_2^* of the interaction well of the second particle. The size of the vibration well L_{vw}^* have a very small influence on the resulting properties. Decreasing elongation L^* increases the critical temperatures and densities. A decreasing size of the second particle σ_2^* in the tangent VSWD produces a large increase in the critical temperature and critical density. An increase in the depth of the interaction well ϵ_2^* produces a large increase in both critical temperature and critical density. Values of $\epsilon_2^*=4$ and 8 show a substantial association phenomena, which produce a decrease in the surface tension γ^*. All series analyzed produce a decrease in the surface tension with respect to the SW and to the tangent homonuclear VSWD in terms of the corresponding state construction. As an ongoing future work, the nature of the association phenomenon found is being studied in depth.

ACKNOWLEDGMENTS

We thank CONACYT for the support given to this work and to the Super Computing Center at UAM-Iztapalapa for a generous allotment of computing time.

[1] J. K. Singh and D. A. Kofke, J. Chem. Phys. **121**, 9574 (2004).
[2] P. Orea, J. Chem. Phys. **123**, 144704 (2005).
[3] F. Sciortino, E. Bianchi, J. F. Douglas, and P. Tartaglia, J. Chem. Phys. **126**, 194903 (2007).
[4] F. Romano, P. Tartaglia, and F. Sciortino, J. Phys.: Condens. Matter **19**, 322101 (2007).
[5] B. J. Alder and T. E. Wainwright, J. Chem. Phys. **31**, 459 (1959).
[6] D. C. Rapaport, J. Chem. Phys. **71**, 3299 (1979).
[7] D. C. Rapaport, J. Comput. Phys. **34**, 184 (1980).
[8] D. J. Tildesley and W. B. Streett, Mol. Phys. **41**, 85 (1980).
[9] G. A. Chapela, S. E. Martinez-Casas, and J. Alejandre, Mol. Phys. **53**,

139 (1984).
[10] G. A. Chapela, S. E. Martinez-Casas, and C. Varea, J. Chem. Phys. **86**, 5683 (1987).
[11] H. S. Gulati and C. K. Hall, J. Chem. Phys. **107**, 3930 (1997).
[12] A. Yethiraj and C. K. Hall, J. Chem. Phys. **95**, 1999 (1991).
[13] A. Yethiraj and C. K. Hall, Mol. Phys. **72**, 619 (1991).
[14] L. Hu, H. Rangwalla, J. Cui, and J. R. Elliott, Jr., J. Chem. Phys. **111**, 1293 (1999).
[15] J. Y. Cui and J. R. Elliott, J. Chem. Phys. **114**, 7283 (2001).
[16] F. A. Escobedo and J. J. de Pablo, J. Chem. Phys. **103**, 2703 (1995).
[17] F. A. Escobedo and J. J. de Pablo, Mol. Phys. **87**, 347 (1996).
[18] S. Kim, J. Chang, and H. Kim, Mol. Phys. **99**, 1023 (2001).
[19] M. Lisal and I. Nezbeda, Mol. Phys. **96**, 335 (1999).
[20] F. W. Tavares, J. Chang, and S. I. Sandler, Fluid Phase Equilib. **140**, 129 (1997).
[21] G. A. Chapela and S. E. Martinezcasas, Mol. Phys. **50**, 129 (1983).
[22] M. P. Taylor, J. Luettmer-Strathmann, and J. E. G. Lipson, J. Chem. Phys. **114**, 5654 (2001).
[23] S. V. Fridrikh and J. E. G.. Lipson, J. Chem. Phys. **116**, 8483 (2002).
[24] J. A. Porter and J. E. G. Lipson, J. Chem. Phys. **122**, 094906 (2005).
[25] G. J. Gloor, G. Jackson, F. J. Blas, E. M. del Rio, and E. de Miguel, J. Phys. Chem. C **111**, 15513 (2007).
[26] L. G. MacDowell and P. Bryk, Phys. Rev. E **75**, 061609 (2007).
[27] G. Jackson, W. G. Chapman, and K. E. Gubbins, Mol. Phys. **65**(1), 1 (1988).
[28] P. Allen and D. J. Tildesley, *Computer Simulations of Liquids* (Oxford University Press, New York, 1987).
[29] P. Orea, J. Lopez-Lemus, and J. Alejandre, J. Chem. Phys. **123**, 114702 (2005).
[30] M. Gonzalez-Melchor, P. Orea, J. Lopez-Lemus, F. Bresme, and J. Alejandre, J. Chem. Phys. **122**, 094503 (2005).
[31] F. Biscay, A. Ghoufi, F. Goujon, V. Lachet, and P. Malfreyt, J. Chem. Phys. **130**, 184710 (2009).
[32] J. Alejandre and G. A. Chapela, J. Chem. Phys. **132**, 014701 (2010).
[33] A. Trokhymchuk and J. Alejandre, J. Chem. Phys. **111**, 8510 (1999).
[34] B. C. Freasier, D. Jolly, and R. J. Bearman, Mol. Phys. **31**, 255 (1976).
[35] P. Orea, Y. Duda, and J. Alejandre, J. Chem. Phys. **118**, 5635 (2003).
[36] J. K. Singh, D. A. Kofke, and J. R. Errington, J. Chem. Phys. **119**, 3405 (2004).
[37] J. R. Elliott and L. Hu, J. Chem. Phys. **110**, 3043 (1999).
[38] P. Orea, Y. Duda, V. C. Weiss, W. Schröer, and J. Alejandre, J. Chem. Phys. **120**, 11754 (2004).